Title	Detrimental Effect of Sintering Additives on Conducting Ceramics: Yttrium‐Doped Barium Zirconate
Author(s)	Han, Donglin; Uemura, Shigeaki; Hiraiwa, Chihiro; Majima, Masatoshi; Uda, Tetsuya
Citation	ChemSusChem (2018), 11(23): 4102‐4113
Issue Date	2018‐12‐11
URL	http://hdl.handle.net/2433/236387
Right	This is the peer reviewed version of the following article: ChemSusChem 2018, 11, 4102 – 4113, which has been published in final form at https://doi.org/10.1002/cssc.201801837. This article may be used for non‐commercial purposes in accordance with Wiley Terms and Conditions for Use of Self‐Archived Versions.; The full‐text file will be made open to the public on 11 December 2019 in accordance with publisher's 'Terms and Conditions for Self‐Archiving'.; This is not the published version. Please cite only the published version.
Type	Journal Article
Textversion	author

Detrimental Effect of Sintering Additives on Conducting Ceramics: Yttrium-Doped Barium Zirconate

Donglin Han [a*], Shigeaki Uemura [b], Chihiro Hiraiwa [b], Masatoshi Majima [b], Tetsuya Uda [a*]

[a] Department of Materials Science and Engineering, Kyoto University,

Yoshida Honmachi, Sakyo-ku, Kyoto 606-8501, Japan

[b] Sumitomo Electric Industries, Ltd.,

1-1-1, Koyakita, Itami-shi, Hyogo 664-0016, Japan

* Corresponding authors: Donglin Han (han.donglin.8n@kyoto-u.ac.jp)

and Tetsuya Uda (uda_lab@aqua.mtl.kyoto-u.ac.jp)

TEL: +81-75-753-5445, FAX: +81-75-753-5284

Abstract

Y-doped BaZrO$_3$ (BZY) is currently the most promising proton conductive ceramic-type electrolyte, showing perspective application in electrochemical devices, including fuel cells, electrolyzer cells. However, due to its refractory nature, sintering additives, such as NiO, CuO or ZnO was commonly added to reduce its high sintering temperature from 1600 $^{\circ}$C to around 1400 $^{\circ}$C. And even without deliberately adding the sintering additive, the NiO anode substrate provides another source of the sintering additive; that is, during the co-sintering process, NiO diffuses from the anode into the BZY electrolyte layer. In this work, we conducted a systematic work to study the effect of NiO, CuO and ZnO on the electroconductive properties of BaZr$_{0.8}$Y$_{0.2}$O$_{3-\delta}$ (BZY20). The results revealed that adding NiO, CuO or ZnO into BZY20, not only degraded the electrical conductivity, but also resulted in enhancement of the hole conduction. Exclusion of these added sintering additives can be realized by post-annealing in hydrogen at the mild temperature of 700 $^{\circ}$C, but kinetically very slow. So, it can be concluded that adding NiO, CuO and ZnO is detrimental to the electroconductive properties of BZY20, and greatly restricts its application as an electrolyte. Developing some new sintering additives, new anode catalysts or new methods for preparing the BZY electrolyte-based cells appears to be urgent.

1. Introduction

Solid oxide fuel cells (SOFCs) using oxide ion-conductive ceramic-type electrolyte, *e.g.*, yttrium-stabilized zirconia (YSZ), possess the highest energy conversion efficiency among various types of fuel cells, but the high operation temperature (typically, > 800 °C) results in great obstacle against their popularization.   Replacing the electrolytes in SOFCs with the proton-conductive types appears to be a promising strategy to reduce the operation temperature [2], since the conduction of protons has relatively lower activation energy than that of the oxide ion conduction, sufficient proton conductivity can be thereby achieved at intermediate temperature range (400 – 700 °C).

Currently, 20 mol% Y-doped $BaZrO_3$ ($BaZr_{0.8}Y_{0.2}O_{3-\delta}$, BZY20) attracts the most attention [3-6], due to its high proton conductivity (*e.g.*, > 0.01 Scm^{-1} at 450 °C [7]), almost pure proton conduction in humid hydrogen atmosphere [8], and excellent chemical stability against reaction with CO_2 [9, 10]. However, the refractory nature of BZY20 requires quite high sintering temperature (at least 1600 °C), leading to significant challenge on its implementation in the fuel cells [11].   Adding sintering additives, such as NiO [12-14], CuO [14, 15], or ZnO [11, 16-18], can reduce the sintering temperature effectively to around 1400 °C, and is already widely adopted to process BZY20.   But, it is worth to note that even without deliberatively introducing sintering additive, NiO in the anode substrate (lately *in-situ* reduced to Ni anode catalyst) provides another source of sintering additive.   As a preliminary examination, we prepared an anode-supported half cell, which has the most common cell configuration composed of a thick BZY20 – 60 wt% NiO anode substrate and a thin BZY20 electrolyte (without

adding any sintering additive) deposited by spin-coating.   After co-sintering at 1500 °C in oxygen for 10 h, the white electrolyte layer turned to be black (**Fig. 1(a)**).   Further analysis on cross-section area (**Fig. 1(b)**) confirms the existence of around 1 at% Ni in the entire dense electrolyte (**Fig. 1(c)**), indicating that the co-sintering process drove NiO to diffuse into the electrolyte layer.   In spite of the recent report by Duan, *et al*., [19], which demonstrated a high performance fuel cell using the BZY20 electrolyte added deliberately with 1 wt% NiO, which showed conductivity remarkably close to 0.01 Scm^{-1} at 600 °C, in most cases, as summarized in **Table 1**, the conductivity of the electrolyte in the co-sintered cells decreased significantly to the range of 0.001 – 0.003 Scm^{-1}.   And the open circuit voltage (OCV) at 600 °C is typically around 0.99 V, obviously lower than the theoretical value about 1.14 V (calculation condition: H_2 – 5% H_2O for anode, and O_2 – 5 H_2O for cathode).   But, such loss in OCV was usually simply attributed to an unsuccessful gas sealing.

Decreasing the sintering temperature by adding NiO, CuO, or ZnO, and co-sintering the NiO anode supported cells are currently the mainstream method to prepare BZY electrolyte-based fuel cells. Although some reports have shown the degradation in electrical conductivity by adding ZnO [11, 16-18] or NiO [33-35], the community still shows insufficient concern on the negative effect on electrical properties by adding these sintering additives.   Especially, as far as we know, there is no report on the effect on the transport properties of BZY20 by adding these oxides, which is another very vital factor restricting the fuel cell performance [36].   Furthermore, a couple of very important information is lack, such as the effect of adding sintering additives on the proton concentration and chemical

expansion of BZY20, which are related to science of the transport properties of BZY and important information for implementing BZY20 electrolyte into the electrochemical devices. And still, it remains as an open question that whether these sintering additives can be removed by post-annealing in reducing atmosphere at moderate temperature. In this work, based on a systematic investigation on three representative sintering additives for BZY20, namely, NiO, CuO and ZnO, we want to emphasise that concern should not be solely placed on their ability to improve the sinterability of BZY20, the negative influence on a couple of fundamental properties of BZY20 should also be considered seriously.

2. Experimental

2.1 Material Preparation

$BaZr_{0.8}Y_{0.2}O_{3-\delta}$ was prepared by a conventional solid state reaction method. Starting materials of $BaCO_3$ (Wako Pure Chemical Industries, Ltd., 99.9%), ZrO_2 (Tosoh Corporation, 98.01%), and Y_2O_3 (Shin-Etsu Chemical Co., Ltd., 99.9%) were mixed at the desired ratio, and ball-milled for 24 h. After being pelletized under 9.8 MPa, the sample was heat-treated at 1000 ℃ for 10 h. Then, the sample was pulverized and ball-milled for 10 h, and pelletized under 9.8 MPa again, with a subsequent heat-treatment at 1300 ℃ for 10 h for synthesizing. After being pulverized and ball-milled for 100 h, the obtained BZY20 powder was mixed with 0.2, 0.5, 1 or 2 wt% NiO (Nikko Rica Corporation, 99.9%), CuO (Nacalai Tesque Inc., 99.9%) or ZnO (Wako Pure Chemical Industries, Ltd., 99.9%), and

subjected to ball-milling for 10 h.　The mixture was then pressed at 392 MPa into pellets with thickness and diameter around 1 mm and 11 mm, respectively.　After being embedded in BZY20 sacrificial powder, the samples were heat-treated at 1500 $^{\circ}$C for 10 h in oxygen atmosphere for sintering.　For comparison, the pure BZY20 powder was also pelletized, embedded in BZY20 – 1 wt% $BaCO_3$ sacrificial powder, and subjected to sintering performed at 1600 $^{\circ}$C for 24 h in oxygen atmosphere.

2.2 Characterization

Chemical compositions were determined by inductively coupled plasma atomic emission spectroscopy (ICP-AES) with SPS4000 (Seiko Instruments Inc., Chiba, Japan).　Microstructures were observed by electron probe microanalyzer (EPMA) with JXA-8530F (JEOL, Tokyo, Japan) and scanning transmission electron microscopy (STEM) with JEOL JEM-2100F.　Wavelength-dispersive X-ray spectroscopy (EPMA-WDS) and energy dispersion X-ray spectroscopy (STEM-EDS, JEOL JED-2300) point analysis was applied to determine the local composition.　Samples for STEM observations were thinned by an argon ion (Ar^+) beam using a JEOL EM-09100IS Ion Slicer.

Powder X-ray diffraction (XRD) measurements were performed using Cu $K\alpha$ radiation with X'Pert PRO MPD (PANalytical, Almelo, Netherland).　High temperature XRD (HT-XRD) measurements were performed using a HTK 1200N high-temperature chamber (Anton Paar, Graz, Austria) attached to the PANalytical X'Pert PRO MPD diffractometer.　Dry or wet ($p_{H_2O} = 0.031$ atm) argon gas was

fed through the high-temperature chamber. HT-XRD patterns were collected during cooling from 1000 to 30 °C at an average cooling rate about 1.06 °Cmin^{-1}. Detailed procedures of HT-XRD measurements were described in our previous work. [37, 38] Rietveld refinement was carried out utilizing a commercial software X'Pert HighScore Plus to determine lattice constants.

Karl-Fischer titration method was applied to determine water content. The pellet-like samples were broken into pieces about 2 mm in length, and hydrated in wet Ar with a water partial pressure of 0.05 atm at desired temperature. Readers are referred to our previous works [39, 40] for detailed procedures.

Ni, Cu or Zn K-edge X-ray absorption near-edge structure (XANES) measurements were performed at the SPring-8 synchrotron radiation facility (Hyogo, Japan) by using a Si(111) double-crystal monochromator at beamlines BL16B2 at 20 K in a vacuum and BL05XU in ambient environment with the approval of the Japan Radiation Research Institute (JASRI) (Proposal No. 2015A5330 and 2017A1797). The samples of BZY20 added nominally with 0.2 wt% NiO, CuO or ZnO were measured in fluorescence mode. Whereas data of reference samples of Ni, Cu or Zn metal, and their binary oxides were collected in transmission mode

2.3 Electrochemical Measurements

Conductivity measurements of the pellet-like samples with sputtered platinum (Pt) electrodes were performed in dry or wet atmosphere of H_2 or O_2. The partial pressure of water vapor in the wet

atmosphere was 0.05 atm.   Pt plates wrapped with silver mesh were used as current collector.   Pt wire was used to lead the current to a frequency response analyzer (Solartron SI 1260, Solartron Analytical, Farnborough, UK).   The impedance spectra were collected in the frequency range from 10 Hz to 7 MHz with applied voltage of 100 mV during cooling from 700 to 100 $^{\circ}$C at 0.2 $^{\circ}$Cmin^{-1}, and were lately analyzed using a commercial software ZView (Scribner Association Inc., NC, USA) Transport numbers of different charge carriers (protons, oxide ions, electronic holes and electrons) in humid hydrogen or oxygen atmospheres were determined by the electromotive force (EMF) method performed at 600 and 700 $^{\circ}$C with the compensated electrode resistance.   Hydrogen concentration cells, oxygen concentration cells, and water vapor concentration cells were established with the EMF values collected.   The partial pressure of water vapor (P_{H_2O}) in the hydrogen and oxygen concentration cells was kept constantly as 0.0312 atm.   And P_{H_2O} in the water vapor concentration cells was 0.0312 and 0.0086 atm at the two opposite electrodes.   The detailed information on the EMF measurements can be found in our previous works [8, 41].   The transport numbers evaluated in the oxygen atmosphere were compensated by taking the effect of electrode polarization into consideration [42, 43].

3. Results

3.1 Composition Analysis and Microstructure Observation of As-Sintered Samples

The actual content of Ni, Cu, and Zn determined by ICP-AES (at%) was plotted against the nominal

content of relevant binary oxide (wt%) in **Fig. 2**.   It should be noted that in this work, both wt% and

at% were used; wt% for the nominal content of NiO, CuO or ZnO, and at% for the actual value of the

cations measured by ICP-AES or STEM-EDS.   From **Fig. 2**, one can see that the actual composition

is lower than the nominal value.   And the loss of Cu and Zn was more serious than Ni, possibly due

to the instability of ZnO (decomposing to $Zn(g)$ and O_2) and higher vapor pressure of $CuO(g)$ at the

sintering temperature (**Fig. S1**).   Then, the as-sintered samples of BZY20 added with 2 wt% NiO,

CuO or ZnO were picked out to check the local composition at intra-grain and grain boundary with

STEM-EDS point analysis (an example is given in **Fig. S2** and **Table S1**).   Since the spot size of the

electron beam of STEM-EDS is about 1 nm, the local composition can be determined precisely.   As

shown in **Table 2**, one can see that the grain boundary area has relatively higher Ni, Cu or Zn content

than that at the intra-grain area.   For example, the Cu content at intra-grain and grain boundary was

0.48 and 2.03 at%, respectively.   The microstructure was observed by EPMA (**Fig. S3**), and in

agreement with the literature; that is, poor sinterability of BZY20 when heated at 1500 $^{\circ}$C for 10 h can

be effectively improved by adding even a small amount (0.2 wt%) sintering additive.

3.2 Hydration Behavior

The proton concentration per unit cell was determined by using Karl-Fischer titration method to

measure the water content in the samples which were heated in Ar – 5% H_2O at desired temperature

for hydration.   As shown in **Fig. 3**, BZY20 without adding any sintering additive shows the highest

proton concentration.   With the increasing temperature and concentration of Ni, Cu or Zn, the proton

concentration decreases.   The results indicate clearly a negative effect on incorporation of protons

into BZY20 by adding NiO, CuO or ZnO.

Then, the HT-XRD measurements were performed in dry oxygen and humid oxygen (p_{H_2O} = 0.031

atm) to collect the information on change of lattice constants with the humidity and amount of sintering

additive.   The lattice constants were determined by Rietveld refinement using a cubic perovskite

model ($Pm\bar{3}m$) [44, 45], and tend to decrease with the increasing amount of NiO, CuO or ZnO, as

shown in **Fig. 4**.   Furthermore, the lattice constants obtained in the wet oxygen atmosphere are larger

than those in the dry atmosphere, indicating a clear chemical expansion effect induced by hydration.

Then, following the approach reported in our previous works [3, 45, 46], a quantitative evaluation on

the effect of chemical expansion was conducted by using Eq. (1), in which $a_{dry\ O_2}$ and $a_{wet\ O_2}$ are the

lattice constants in dry and wet oxygen atmosphere, respectively.   As shown in **Fig. 5**, the change

ratio of lattice constant increases with the increasing proton concentration, and decreases with the

increasing content of Ni, Cu and Zn.   It is quite reasonable, since the chemical expansion is induced

by hydration which incorporates protons, whereas increasing the amount of NiO, CuO or ZnO results

in a reduction in the capability for proton incorporation.

$$change\ ratio\ of\ lattice\ constant = \frac{a_{wet\ O_2} - a_{dry\ O_2}}{a_{dry\ O_2}} \times 100\ \% \qquad (1)$$

3.3 Electrical Conductivity

The electrical conductivity was determined by analysing the impedance spectra, which were collected through three continuous cycles in different atmosphere. Since the samples were sintered in the oxygen atmosphere, the first cycle was performed in wet O_2 during cooling from 700 ^oC to 100 ^oC after the conductivity was stabilized at 700 ^oC. Then, the samples were annealed at 700 ^oC in wet H_2 for 10 h, followed by a subsequent running of the second cycle. Finally, the atmosphere was altered to wet O_2 again for the third cycle. Through such designed sequence, not only the dependence of the conductivity on the amount of sintering additives, but also the redox properties of the samples can be revealed.

The impedance spectra of the samples added nominally with 0.5 wt% NiO, CuO or ZnO are given in **Fig. 6** for example. The semi-circles appear at the high and middle frequency ranges are attributed to the resistance from bulk (intra-grain) and grain boundary, respectively, judged from their specific capacitance around 10^{-11} and 10^{-9} F, respectively [3, 47]. By taking the geometric factors (thickness and area) into consideration, the bulk, grain boundary, and total conductivities were determined (see Electronic Supplementary Information for Arrhenius plots). Since in most cases, the semicircles belonging to the bulk and grain boundary resistances are only distinguishable up to around 300 ^oC (an example of BZY20 – 0.5 wt% NiO is given in **Fig. S4**), for the sake of comparison, the bulk and grain boundary conductivities at 300 ^oC are picked out and plotted in **Figs. 7** and **8**, respectively. The temperature of 300 ^oC is selected because transport number of proton at such low temperature is close

to unity according to the EMF measurement in the later section.

As shown in **Fig. 7**, the bulk conductivity measured at 300 $^{\circ}$C in the first cycle in wet O_2, in general, decreased with the increasing cation ratio of Ni, Cu or Zn, which indicates clearly a negative effect on the bulk conductivity by adding NiO, CuO or ZnO.   When the atmosphere was altered to wet H_2 (the second cycle), reduction in bulk resistance (**Fig. 7**), and correspondingly, enhancement in bulk conductivity were observed.   Especially, in the case of adding CuO (**Fig. 7(b)**), the bulk conductivity in wet H_2 is even higher than that of the pure BZY20.   After the atmosphere was returned to wet O_2 again (the third cycle), the conductivity decreased, but are still obviously higher than that measured in the first cycle in wet O_2.

The behaviour of grain boundary conductivity at 300 $^{\circ}$C (**Fig. 8**) is relatively complicated, since there is no clear relationship in the magnitude among different cycles.   For example, for the samples added with NiO, the grain boundary conductivity measured in the first cycle in wet O_2 is the highest, but for the CuO or ZnO-added samples, the highest grain boundary conductivity was obtained in the second cycle in wet H_2.   However, qualitatively, the grain boundary conductivity also tends to decrease with the increasing cation ration of Ni, Cu or Zn, and is apparently smaller than the bulk conductivity.

The total conductivity at 600 $^{\circ}$C, which is typical temperature for fuel cell operation, is shown in **Fig. 9**.   The total conductivity also shows the tendency to decrease with the increasing amount of NiO, CuO or ZnO additives.   At 600 $^{\circ}$C, the contribution of hole conduction is enhanced [8, 48], and the conductivities in wet O_2 in some samples are relatively higher than that measured in wet H_2.

3.4 Transport Numbers

The EMF method was applied to determine the transport numbers of various charge carriers, including protons, oxide ions, and electronic holes in the samples added with 2 wt% NiO, CuO or ZnO. The voltage measured in the hydrogen concentration cells are very close to the Nernst voltage, indicating that regardless of NiO, CuO or ZnO additive, almost pure ionic conduction (protons and oxide ions) occurred (**Fig. S16**). However, in the mode of oxygen concentration cells, the measured voltage is obviously lower than the Nernst voltage (**Fig. S17**), implying generation of significant contribution of hole conduction. Here, compensation was performed in wet oxidizing atmosphere by taking the electrode polarization effect into consideration [8, 42].

As shown in **Fig. 10**, regardless of whether NiO, CuO or ZnO was added into BZY20, almost pure ionic conduction, mainly proton conduction, occurred in hydrogen atmosphere. However, when exposing to the oxygen atmosphere, even in the case of pure BZY20, the transport number of ionic conduction deviates obviously from unity. And further reduction in the contribution of the ionic conduction was confirmed by adding the sintering additives. For example, the transport number of ionic conduction at 600 $^{\circ}$C in the pure BZY20 sample is about 0.69, but decreased greatly to 0.34, 0.39 and 0.43, when 2 wt% NiO, CuO and ZnO was added, respectively. These results definitely show negative impact on the ionic conduction in BZY20 when NiO, CuO or ZnO was added.

Such enhancement in the contribution of hole conduction might correlate with the decreased capability for proton introduction. The protons are incorporated into barium zirconate through hydration

reaction given in Equation (2). However, as shown in Figure 3, the proton concentration decreased with the increasing Ni concentration, indicating that less oxide ion vacancies ($V_O^{\bullet\bullet}$) participate in the hydration reaction and are available for the reaction given in Equation (3) to form electronic holes ($h^\bullet$). However, the hole conduction was influenced not only by the concentration, but also the mobility of the holes, which might also change when these sintering additives were added.

$$H_2O + V_O^{\bullet\bullet} + O_O^\times = 2OH_O^\bullet \tag{2}$$

$$O_2 + 2V_O^{\bullet\bullet} = 2O_O^\times + 4h^\bullet \tag{3}$$

3.5 Post-Annealing in Hydrogen

Since NiO, CuO and ZnO influence negatively the capability of proton incorporation and electrical properties of BZY20, whether they can be excluded, for example, by post-annealing in reducing atmosphere, appears to be an interesting and meaningful topic. Our previous work on the BZY20-NiO system shows that Ni cations, possibly taking trivalent state, incorporate into the cubic perovskite crystal structure of BZY20, and mainly occupy an interstitial position between two adjacent Ba cations, resulting in formation of Ba vacancies due to the electrostatic repulsion [33]. These Ni cations can be entirely excluded to the grain boundary of BZY20 in the form of Ni metal particles by annealing at 1400 °C in Ti-deoxidized Ar atmosphere, but can hardly be excluded at 600 °C in pure hydrogen [34]. Meanwhile, Nasani, *et al.* [49] and Polfus *et al.* [50] found that the exclusion of nickel can be partially realized in hydrogen at relatively higher temperature, such as 750 and 800 °C. Here, at the annealing

temperature of 700 °C in this work, we want to see whether the same exclusion phenomenon can occur, especially in the system added with CuO or ZnO, which was not reported.

Firstly, the samples of BZY20 added with 2 wt% NiO, CuO or ZnO were annealed in dry H_2 at 700 °C for 48 h, then subjected to STEM-EDS point analysis to determine the local composition in intra-grain and grain boundary area with the results summarized in **Table 2**. For the BZY20 – 2 wt% NiO sample, the Ni cation ratio in the intra-grain and grain boundary area is 1.92 and 2.34 at%, respectively, close to the values of 1.93 and 2.50 at% for the as-sintered sample (1500 °C, O_2,10h). The case of the BZY20 – 2 wt% ZnO sample is similar. However, the sample added with 2 wt% CuO behaves differently; that is, the Cu cation ratio in the intra-grain and grain boundary area of the as-sintered sample is about 0.48 and 2.03 at%, and decreases greatly to 0.24 and 0.38 at%, respectively, after annealing in H_2 at 700 °C. We suppose that Cu metal particles might segregate at the grain boundary of BZY20 as a consequence. However, possibly due to the very small area available for TEM observation, we were unable to confirm the segregation of any Cu metal particle.

The analysis on the 2 wt% NiO, CuO or ZnO-contained samples only indicates that copper can be effectively excluded from BZY20. Then we carried out XANES measurement to confirm existence of metal copper. XANES measurements on the samples containing reduced amount, *i.e.* 0.2 wt%, of NiO, CuO or ZnO, provided additional interesting information. As shown in **Fig. 11**, the XANES spectra of all the as-sintered samples are obviously different from those of the corresponding reference samples, implying that most of NiO, CuO or ZnO incorporated successfully into the crystal structure

of BZY20, rather than remained as their binary oxides.   But, after annealing in hydrogen at 700 ℃

for 48 h, the spectrum of BZY20 – 0.2 wt% NiO turns to be close to that of Ni metal.   The spectrum

of BZY20 – 0.2 wt% CuO also changed, and is obviously different from that of CuO.   It is difficult

to determine whether the spectrum is close to Cu or Cu_2O.   But, since the spectrum shifted towards

the low energy side, it is definite that the oxidation state of Cu cations is reduced.   However, the

spectrum of BZY20 – 0.2 wt% ZnO does not change much from that of the as-sintered one.

4. Discussion

4.1 Exclusion of nickel and copper from intra-grain of BZY20 and correlation with conductivity

Evidently, it can be concluded that copper and nickel are available to be excluded from BZY20 after

post-annealing at 700 ℃ in hydrogen.   And the exclusion of copper seems to be much more

kinetically favourable, since clear decrease of the Cu concentration at both the intra-grain and grain

boundary area was confirmed in the post-annealed BZY20 – 2 wt% CuO sample.   Comparably,

exclusion of nickel appears to be more difficult.   In our previous work [33], post-annealing the

BZY20 sample containing about 0.40 at% Ni at 600 ℃ in hydrogen for 24 h only results in a slight

shift in the Ni K-edge XANES spectra without obvious change in the shape of the spectra (also plotted

in **Fig. 11(a)** for comparison).   But in this work, annealing the BZY20 – 0.2 wt% NiO (0.39 at% Ni

by ICP-AES) sample at higher temperature of 700 ℃ for longer time of 48 h leads to the XANES

spectrum approaching to the metal Ni reference, but notably, not entirely the same as the Ni reference,

indicating that a part of nickel incorporated into BZY20 remained in the oxide structure. However, we did not observe clear change in intra-grain Ni concentration in the BZY20 – 2 wt% NiO sample before and after the post-annealing in hydrogen. One possible reason might be attributed to the different grain size of BZY20 achieved by adding different amount of NiO; about 1 μm for BZY20 – 0.2 wt% NiO, whereas larger than 5 μm for BZY20 – 2 wt% NiO. The larger grain size needs longer time for nickel to be obviously excluded from the intra-grain, which is actually a diffusion process. Furthermore, partial exclusion of nickel was reported by annealing NiO-added $BaZr_{0.85}Y_{0.15}O_{3-\delta}$ (grain size around 3 μm) at higher temperature of 750 [49] and 800 ^{o}C [50] for 15 and 24 h, respectively. So, it can be concluded that nickel can be excluded from barium zirconate at such mild temperature, but the process is kinetically slow. Entire exclusion of nickel might require quite high temperature or long time, for example, 1400 ^{o}C for 100 h in the Ti-deoxidized Ar atmosphere as reported in our previous work [34].

The electrical conductivity no doubt will be influenced by the annealing in hydrogen with consequent exclusion of nickel and copper. One can see that after annealing the samples added with NiO or CuO at 700 ^{o}C in wet hydrogen for 10 h during the second cycle for conductivity measurement, the bulk conductivity increased over that of the first cycle in wet oxygen. But, exclusion of nickel or copper is not the only reason for the recovery of bulk conductivity. Since nickel incorporated into the crystal structure of barium zirconate takes the form of trivalent nickel cations [33], exposure to hydrogen will thereby reduce a part of these trivalent nickel cations ($Ni_i^{\cdot\cdot}$) to lower valence state, such as divalent

($Ni_i^{\cdot\cdot}$), or perhaps to metallic state with incorporating proton into bulk and changing the activation energy to favour the migration of protons. Further exposure to the oxygen atmosphere (the third cycle) causes the nickel cations return to the trivalent state. The conductivity decrease in consequence, but will not completely return to the value collected at the first cycle in oxygen, because a part of nickel has already been excluded from barium zirconate. Of course, the extent of returning of the conductivity is different with the grain size. Such behaviour of conductivity obtained among different cycles is quite clear in the sample with high amount of NiO additive, *e.g.*, 2 wt% (**Fig. S5(d)**). The conductivity behaviour of the samples added with CuO appears to be similar, however, the bulk conductivity measured in the wet hydrogen atmosphere increased surprisingly, even higher than that of the pure BZY20. The reason is not clear, but one hypothesis is that in the reducing atmosphere, in addition to be excluded as copper metal, a part of the copper cations might be reduced to lower valences state, such as from Cu(II) to Cu(I), resulting in a local lattice expansion surrounding these copper cations because generally, tensional stress on barium zirconate benefits the proton conduction [51]. However, such hypothesis needs further investigation in future.

In the case of the samples added with ZnO, we also observed a clear enhancement in the bulk conductivity when the atmosphere was altered from wet oxygen (the first cycle) to wet hydrogen (the second cycle). But the composition changes in the BZY20 – 2 wt% ZnO sample is little and the spectrum of BZY20 – 0.2 wt% ZnO does not change so much in hydrogen. At present, we do not have any hypothesis to explain these behaviours clearly.

4.2 Current Fabrication Method of Anode-Supported Cells and Perspective

Currently, the most common structure for BZY20 electrolyte-based cells is the anode-supported one

coupled with the co-sintering process with the sintering additive optionally added, which allows the

implementation of the electrolyte layers thinned to be tens of micrometers with minimized loss in

ohmic resistance. In fact, not only fuel cells, but also some other electrochemical devices, including

cells of electrolyzer [52, 53], hydrogen separation [54, 55] and methane reforming [56, 57], were

fabricated with such method. However, as clarified in our preliminary experiment (**Fig. 1**), regardless

of whether sintering additives were added on purpose or not, NiO in the anode diffuses into the

electrolyte layer and plays the role of the sintering additive. Reviewing the literature reveals that the

co-sintered cells have the conductivity around 0.001 to 0.003 Scm^{-1} (**Table 1**), in accordance with the

results in this work; that is, the BZY20 sample added with 1 or 2 wt% NiO shows the conductivity

(mainly proton conduction) lower than 0.004 Scm^{-1} in wet hydrogen (**Fig. 9**). Furthermore, the open

circuit voltage values are all not higher than 1.01 V, obviously lower than the Nernst voltage around

1.14 V, which is a direct result from the enhanced hole conduction in BZY20 affected by adding NiO,

CuO or ZnO. It is worth to note that people may mistakenly expect that the hole conduction in

BZY20 electrolyte generated at the cathode side can be blocked by the anode side. But actually,

chemical potential of oxygen does not linearly distribute across the electrolyte. It keeps high to the

vicinity of the anode side, and drops dramatically [36]. So, even BZY20 shows pure ionic conduction

in hydrogen, the leakage current generated due to the hole conduction can not be ignored.

Considering the case of a co-sintered fuel cell, which has an electrolyte layer with the thickness and conductivity typically of 25 μm and 0.002 Scm^{-1}, respectively, the pure BZY20 electrolyte (proton conductivity around 0.01 Scm^{-1}) showing comparable performance will be allowed to be thicker for 5 times (namely, 125 μm) but even with less hole conduction.   So, strategy of adding these sintering additives, or co-sintering a NiO anode stood cell faces quite severe challenge to improve the cell performance, and it appears to be meaningless if one still uses the co-sintering method to develop the NiO anode-supported fuel cells with the BZY electrolyte.

Reports on using pulsed laser deposition (PLD) method to prepare the BZY electrolyte provide a clear and attractive image on how well the fuel cells should perform with a pure BZY electrolyte, since the PLD method is able to directly deposit dense BZY electrolyte layer with good crystallinity.   Pergolesi, *et al.* [21] reported a fuel cell with 4 μm thick BZY20 electrolyte, showing the peak power density of 110 mWcm^{-2} at 600 $^{\circ}$C.   Recently, Bae, *et al.* [30] demonstrated a high performance fuel cell with a PLD-prepared thin BaZr$_{0.85}$Y$_{0.15}$O$_{3-\delta}$ (BZY15) electrolyte deposited on a BZY15 – 56 wt% NiO anode. The peak power density achieved remarkably 740 mWcm^{-2} at 600 $^{\circ}$C, and they attributed such great improvement only to successfully thinning the electrolyte to 2.5 μm.   But another important reason should be the success in preparing the thin electrolyte layer without NiO.   According to this study, eliminating NiO from the electrolyte leads high OCV and high proton conductivity.   In fact, relatively high OCV were reported.   However, we need discussion about the conductivity. Using the ohmic resistance and thickness of the electrolyte layer, the conductivity of the BZY20 and BZY15 electrolyte

layers in the works of Pergolesi, *et al*. [21] and Bae, *et al*. [30] is estimated to be 0.00021 and 0.00278 Scm^{-1}, respectively.   But these values are about one tenth small in comparison with the conductivity of the pellet sample.   One of reason might be off stoichiometry and another reason is ohmic resistance in electrode layers.   The anode substrate in the work of Pergolesi, *et al*. [21] contains only 26 wt% NiO, far from the appropriate NiO content about 40 – 70 wt% [58, 59].   And Bae, *et al*. [30] inserted a functional layer composed of nano-sized BZY15 and NiO particles between the electrolyte and anode layers.   Therefore, the measured ohmic resistance may not reflect solely the contribution from the electrolyte layer.   At present, the PLD method is still high cost, and not available to deposit thin films with large scale. [60]   In addition to such problems, the process to apply PLD on depositing BZY also needs to be optimized for fuel cell application.

In our opinion, to further develop the anode-supported fuel cells with the BZY electrolyte, some new discovery and technology for processing is essential.   For example, finding a new sintering additive which is not detrimental to the electroconductive properties of BZY, developing an alternative anode material which does not react with BZY during the co-sintering, or designing a cost-effective new process which does not need the co-sintering step, or does not induce the reaction between BZY and NiO.   At least, the negative effect on adding the sintering additives of NiO, CuO and ZnO, and also the problem on diffusion of NiO into the electrolyte during the co-sintering, should be sufficiently recognized.

5. Conclusions

In this work, a systematic investigation was performed to study the effect of NiO, CuO and ZnO on the electroconductive properties of $BaZr_{0.8}Y_{0.2}O_{3-\delta}$ (BZY20).　The results revealed that although adding these oxides improved the sinterability of BZY20, significant reduction in capability of proton incorporation and proton conductivity occurred, together with enhancement in hole conduction.　The added NiO, CuO or ZnO sintering additive can be, in some cases, lately excluded out of BZY20 by post-annealing in the hydrogen atmosphere at mild temperature, such as 700 $^{\circ}$C, but such process is kinetically slow.　Therefore, in conclusion, adding NiO, CuO and ZnO imposes detrimental impact on the electroconductive properties of BZY20, thereby restricts its application as sintering additives. It is worth to note that, even without deliberately adding these sintering additives, NiO in the anode also diffuses into the BZY20 electrolyte layer, and plays the same role as the sintering additive.　So, developing new sintering additives, new anode catalysts or new processing for preparing the BZY electrolyte-based cells is an urgent task.

References

[1] B.C.H. Steele, A. Heinzel, *Nature* **2001**, *414*, 345 - 352.

[2] A. Dubois, S. Ricote, R.J. Braun, *J. Power Sources* **2017**, *369*, 65 - 77.

[3] D. Han, K. Shinoda, S. Sato, M. Majima, T. Uda, *J. Mater. Chem. A* **2015**, *3*, 1243 - 1250.

[4] D. Han, N. Hatada, T. Uda, *J. Am. Ceram. Soc*. **2016**, *99*, 3745 - 3753.

[5] E. Gilardi, E. Fabbri, L. Bi, J.L.M. Rupp, T. Lippert, D. Pergolesi, E. Traversa, *J. Phys. Chem. C*, **2017**, *121*, 9739 - 9747.

[6] D. Pergolesi, E. Fabbri, A. D'Epifanio, E.D. Bartolomeo, A. Tebano, S. Sanna, S. Licoccia, G. Balestrino, E. Traversa, *Nat. Mater*. **2010**, *9*, 846 - 852.

[7] Y. Yamazaki, R. Hernandez-Sanchez, S.M. Haile, *Chem. Mater*. **2009**, *21*, 2755 - 2762.

[8] D. Han, Y. Noda, T. Onishi, N. Hatada, M. Majima, T. Uda, *Int. J. Hydrogen Energy* **2016**, *41*, 14897 - 14908.

[9] K. Kato, D. Han, T. Uda, *J. Am. Ceram. Soc*. **2018**, doi: 10.1111/jace.15946.

[10] K. Katahira, Y. Kohchi, T. Shimura, H. Iwahara, *Solid State Ionics* **2000**, *138*, 91 - 98.

[11] Y. Guo, Y. Lin, H. Shi, R. Ran, Z. Shao, *Chin, J. Catal.* **2009**, *30*, 479 - 481.

[12] P. Babilo, S.M. Haile, *J. Am. Ceram. Soc.* **2005**, *88*, 2362 - 2368.

[13] J. Tong, D. Clark, M. Hoban, R. O'Hayre, *Solid State Ionics* **2010**, *181*, 496 - 503.

[14] J. Tong, D. Clark, L. Bernau, M. Sanders, R. O'Hayre, *J. Mater. Chem*. **2010**, *20*, 6333 - 6341.

[15] S. Nikodemski, J. Tong, R. O'Hayre, *Solid State Ionics* **2013**, *253*, 201 - 210.

[16] K. Park, Y. Seo, K.B. Kim, S. Song, B. Park, J. Park, *J. Alloy. Compd.* **2015**, *639*, 435 - 444.

[17] S. Tao, J.T.S. Irvine, *Adv. Mater.* **2006**, *18*, 1581 - 1584.

[18] S. Tao, J.T.S. Irvine, *J. Solid State Chem.* **2007**, *180*, 3493 - 3503.

[19] J.T.S. Irvine, A. Kruth, C.D. Savaniu, S. Tao, Steam Electrolysis, US Pat., 7906006B2, 2011(filing date Mar.24, 2005).

[20] C. Duan, J. Tong, M. Shang, S. Nikodemski, M. Sanders, S. Ricote, A. Almansoori, R. O'Hayre, *Science* **2015**, *349*, 1321 - 1326.

[21] C. Duan, R.J. Kee, H. Zhu, C. Karakaya, Y. Chen, S. Ricote, A. Jarry, E.J. Crumlin, D. Hook, R. Braun, N.P. Sullivan, R. O'Hayre, *Nature* **2018**, *557*, 217-222.

[22] W. Sun, L. Yan, Z. Shi, Z. Zhu, W. Liu, *J. Power Sources* **2010**, *195*, 4727 - 4730.

[23] D. Pergolesi, E. Fabbri, E. Traversa, *Electrochem. Commun.* **2010**, *12*, 977 - 980.

[24] E. Fabbri, L. Bi, H. Tanaka, D. Pergolesi, E. Traversa, *Adv. Func. Mater.* **2011**, *21*, 158 - 166.

[25] L. Bi, E. Fabbri, Z. Sun, E. Traversa, *Energy Environ. Sci.* **2011**, *4*, 1352 - 1357.

[26] Z. Sun, E. Fabbri, L. Bi, E. Traversa, *J. Am. Ceram. Soc.* **2012**, *95*, 627 - 635.

[27] J. Xiao, W. Sun, Z. Zhu, Z. Tao, W. Liu, *Mater. Lett.* **2012**, *73*, 198 - 201.

[28] I. Luisetto, S. Licoccia, A. D'Epifanio, A. Sanson, E. Mercadelli, E.D. Bartolomeo, *J. Power Sources* **2012**, *220*, 280 - 285.

[29] Y. Liu, Y. Guo, R. Ran, Z. Shao, *J. Membr. Sci.* **2012**, *415 - 416*, 391 - 398.

[30] W. Sun, Z. Shi, M. Liu, L. Bi, W. Liu, *Adv. Func. Mater.* **2014**, *24*, 5695 - 5702.

[31] S.P. Shafi, L. Bi, S. Boulfrad, E. Traversa, *J. Electrochem Soc*. **2015**, *162*, F1498 – F1503.

[32] K. Bae, D.Y. Jang, H.J. Choi, D. Kim, J. Hong, B. Kim, J. Lee, J. Son, J.H. Shim, *Nat. Commun.* **2017**, 14553.

[33] L. Bi, E.H. Da'as, S.P. Shafi, *Electrochem. Commun*. **2017**, *80*, 20 - 23.

[34] H. Dai, *Ceram. Int*. **2017**, *43*, 7362 - 7365.

[35] D. Han, K. Shinoda, S. Tsukimoto, H. Takeuchi, C. Hiraiwa, M. Majima, T. Uda, *J. Mater. Chem. A* **2014**, *2*, 12552 - 12560.

[36] D. Han, J. Iihara, S. Uemura, K. Kazumi, C. Hiraiwa, M. Majima, T. Uda, *J. Mater. Chem. A*. **2016**, *4*, 10601 - 10608.

[37] N. Nasani, D. Pukazhselvan, A.V. Kovalevsky, A.L. Shaula, D.P. Fagg, *J. Power Sources* **2017**, *339*, 93 - 102.

[38] T. Nakamura, S. Mizunuma, K. Yamauchi, K. Mikami, T. Kuroha, K. Amezawa, *18th International Conference on Solid State Protonic Conductors*, Oslo, Norway, **2016**.

[39] C. Hiraiwa, D. Han, A. Kuramitsu, A. Kuwabara, H. Takeuchi, M. Majima, T. Uda, *J. Am. Ceram. Soc*. **2013**, *96*, 879 - 884.

[40] D. Han, M. Majima, T. Uda, *J. Solid State Chem.* **2013**, *205*, 122 - 128.

[41] D. Han, Y. Okumura, Y. Nose, T. Uda, *Solid State Ionics* **2010**, *181*, 1601 - 1606.

[42] D. Han, Y. Nose, K. Shinoda, T. Uda, *Solid State Ionics* **2012**, *213*, 2 - 7.

[43] K. Shitara, T. Moriasa, A. Sumitani, A. Seko, H. Hayashi, Y. Koyama, R. Huang, D. Han, H.

Moriwake, I. Tanaka, *Chem. Mater.*, 2017, **29**, 3763.

[44] M. Liu, H. Hu, *J. Electrochem. Soc.* **1996**, *143*, L109 – L112.

[45] V.V. Kharton, F.M.B. Marques, *Solid State Ionics* **2001**, *140*, 381 - 394.

[46] D. Han, K. Kishida, K. Shinoda, H. Inui, T. Uda, *J. Mater. Chem. A* **2013**, *1*, 3027 - 3033.

[47] D. Han, K. Shinoda, T. Uda, *J. Am. Ceram. Soc*. **2014**, *97*, 643 - 650.

[48] D. Han, K. Kato, T. Uda, *Chem. Comm*. **2017**, *53*, 12684 - 12687.

[49] S.M. Haile, D.L. West, J. Campbell, *J. Mater. Res*. **1998**, *13*, 1576 - 1595.

[50] K. Nomura, H. Kageyama, *Solid State Ionics* **2007**, *178*, 661 - 665.

[51] J.M. Polfus, M. Fontaine, A. Thøgersen, M. Riktor, T. Norby, R. Bredesen, *J. Mater. Chem. A* **2016**, *4*, 8105 - 8112.

[52] A. Fluri, A. Marcolongo, V. Roddatis, A. Wokaun, D. Pergolesi, N. Marzari, T. Lippert, *Adv. Sci*. **2017**, 1700467.

[53] L. Bi, S.P. Shafi, E. Traversa, *J. Mater. Chem. A* **2015**, *3*, 5815 - 5819.

[54] L. Lei, Z. Tao, X. Wang, J.P. Lemmon, F. Chen, *J. Mater. Chem. A* **2017**, *5*, 22945 - 22951.

[55] S. Fang, S. Wang, K.S. Brinkman, F. Chen, *J. Mater. Chem. A* **2014**, *2*, 5825 - 5833.

[56] S. Fang, S. Wang, K.S. Brinkman, Q. Su, H. Wang, F. Chen, *J. Power Sources* **2015**, *278*, 614 - 622.

[57] S.H. Morejudo, R. Zanón, S. Escolástico, I. Yuste-Tirados, M. Malerød-Fjeld, P.K. Vestre, W.G. Coors, A. Martínez, T. Norby, J.M. Serra, C. Kjølseth, *Science*, **2016**, *353*, 563 - 566.

[58] H. Malerød-Fjeld, D. Clark, I. Yuste-Tirados, R. Zanón, D. Catalán-Martinez, D. Beeaff, S.H. Morejudo, P.K. Vestre, T. Norby, R. Haugsrud, R.; J.M. Serra, C. Kjølseth, *Nat. Energy* **2017**, *2*, 923 - 931.

[59] L. Bi, E. Fabbri, Z. Sun, E. Traversa, *J. Electrochem. Soc.* **2011**, *158*, B797 – B803.

[60] T. Onishi, D. Han, Y. Noda, N. Hatada, M. Majima, T. Uda, *Solid State Ionics* **2018**, *317*, 127 - 135.

[61] E. Stefan, M. Stange, C. Denonville, Y. Larring, N. Hildenbrand, T. Norby, R. Hausgrud, *J. Mater. Sci*. **2017**, *52*, 6486 - 6497.
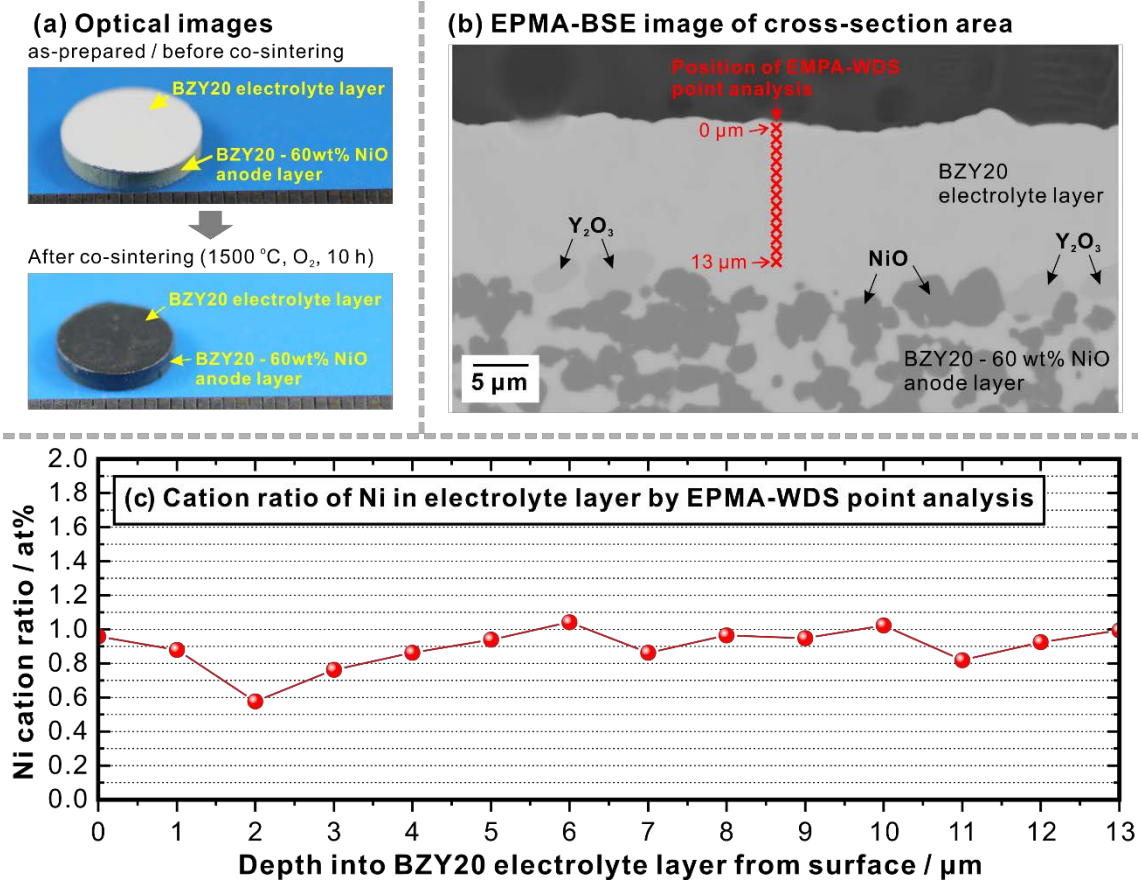
Fig. 1 Preliminary examination on a half cell composed of a BZY20 – 60 wt% NiO anode layer and a spin-coated BZY20 electrolyte layer. (a) Optical images showing the electrolyte layer turned to be black color after co-sintering at 1500 °C in oxygen atmosphere for 10 h. (b) An EPMA back scattering electron (EPMA-BSE) image of the cross-section area (polished by JEOL IB-19510CP Cross Section Polisher). (c) Cation ratio of Ni in the electrolyte layer by performing EPMA-WDS point analysis on the position marked with cross symbols in (b).
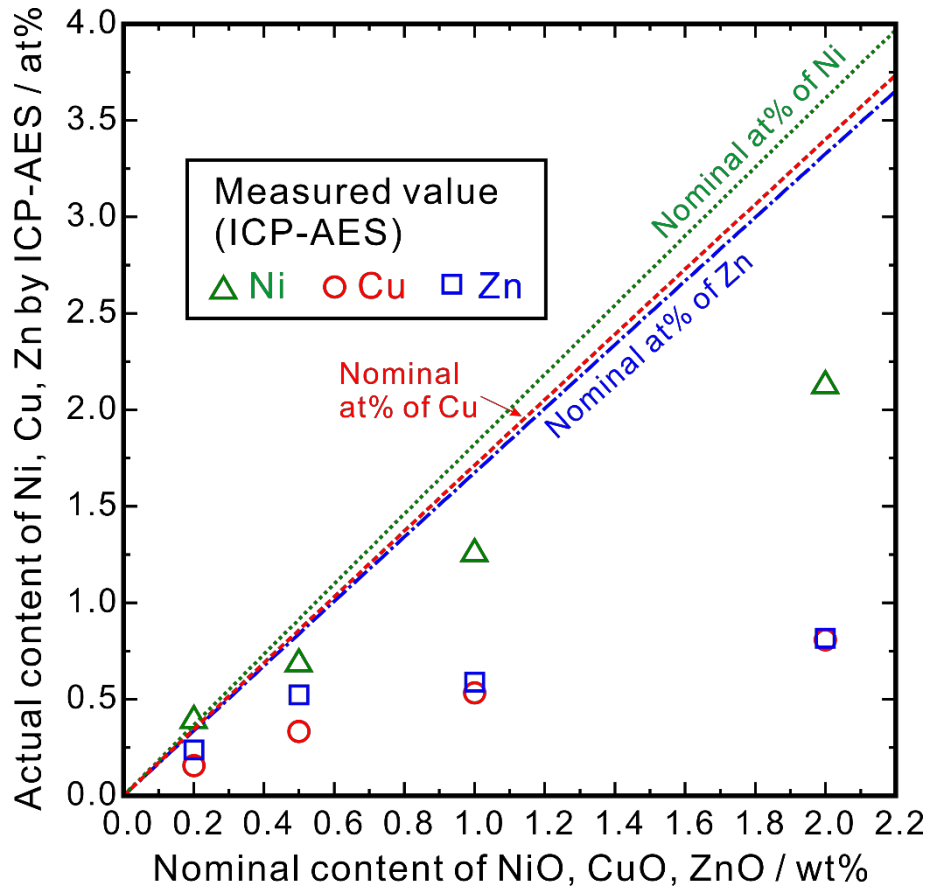
Fig. 2 Actual composition of Ni, Cu, Zn in the as-sintered samples determined by ICP-AES measurements plotted against the nominal content of NiO, CuO, ZnO added into BZY20. The samples were heat-treated at 1500 ºC in O_2 for 10 h for sintering.
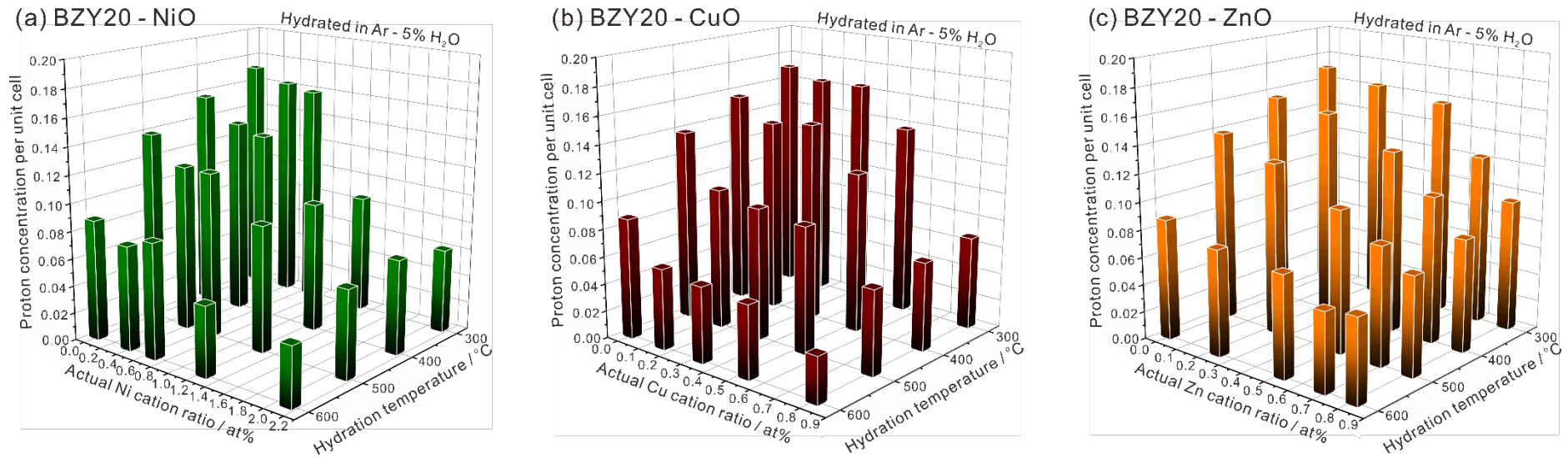
Fig. 3 Proton concentration of BZY20 added with various content of NiO, CuO or ZnO, plotted against the actual cation ratio of Ni, Cu or Zn measured by ICP-AES.   The samples were sintered at 1500 °C in oxygen for 10 h, and hydrated in Ar – 5% H$_2$O.   The proton concentration was calculated from water content measured by Karl-Fischer titration method.
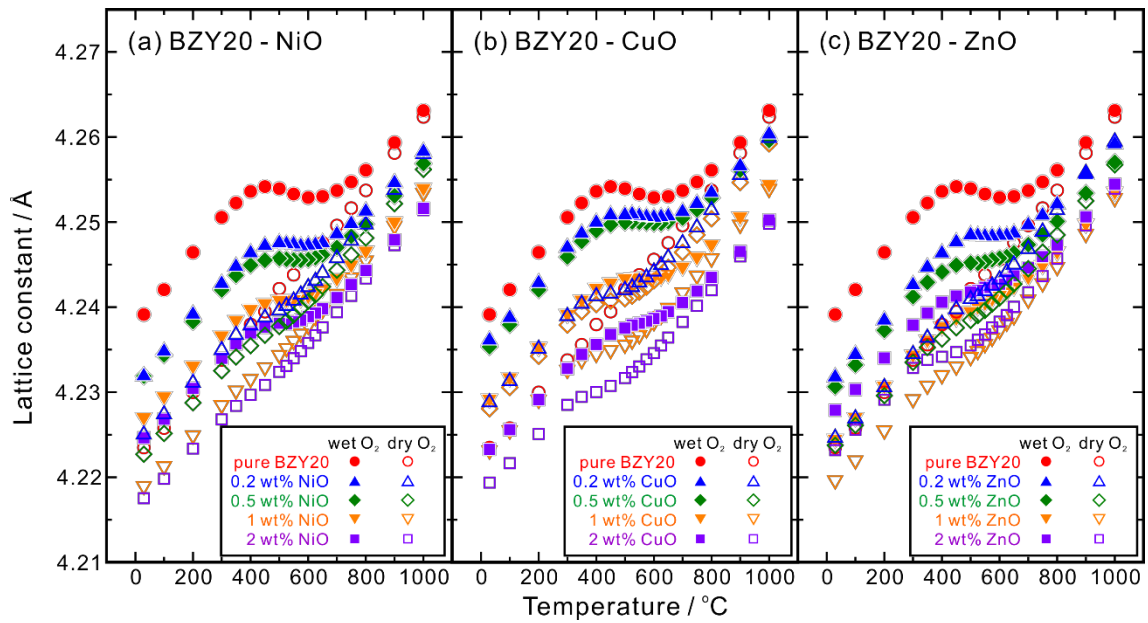
Fig. 4 Temperature dependence of lattice constants of BZY20 added with various content of NiO, CuO or ZnO in dry or wet O_2 ($p_{H_2O} = 0.031\,atm$) atmosphere. All the samples were finally heat-treatment at 1500 ^{o}C in O_2 for 10 h for sintering. The profile of pure BZY20 [3] is also plotted for comparison.
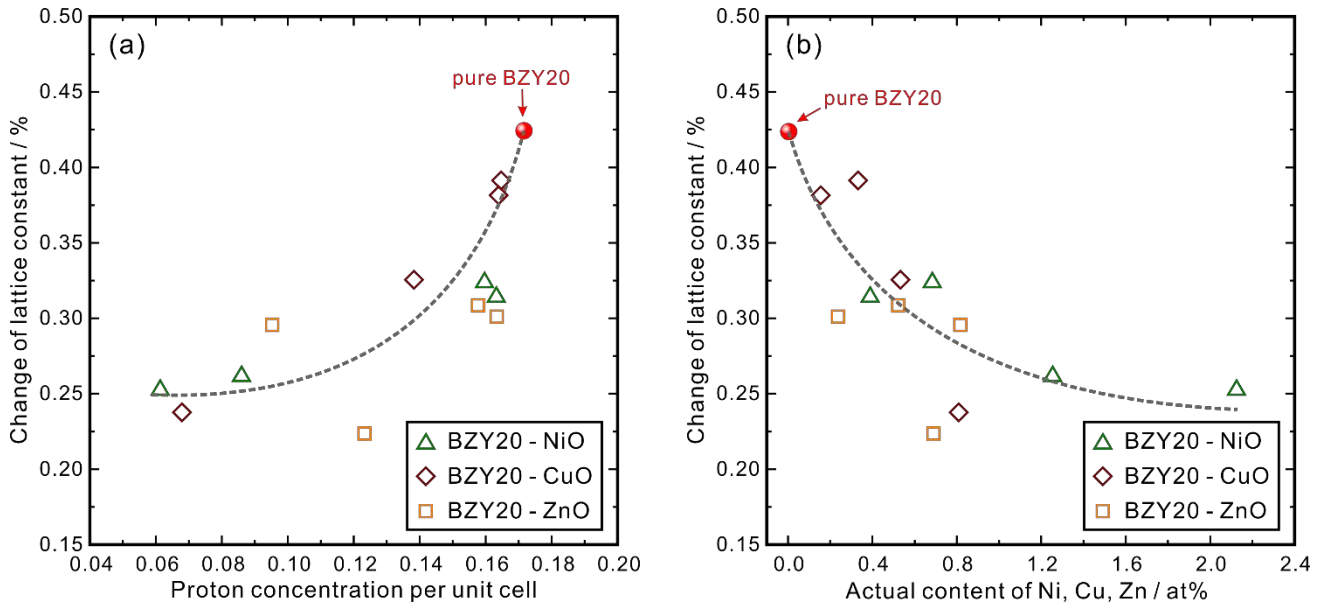
Fig. 5 Change of lattice constant of BZY20 added with various content of NiO, CuO or ZnO due to hydration plotted against (a) proton concentration, and (b) actual cation ratio of Ni, Cu, Zn measured by ICP-AES. All the samples were prepared by heat-treating at 1500 ^{o}C in O_2 for 10 h for sintering. The data of pure BZY20 which was sintered at 1600 ^{o}C in O_2 for 24 h was also plotted for comparison.
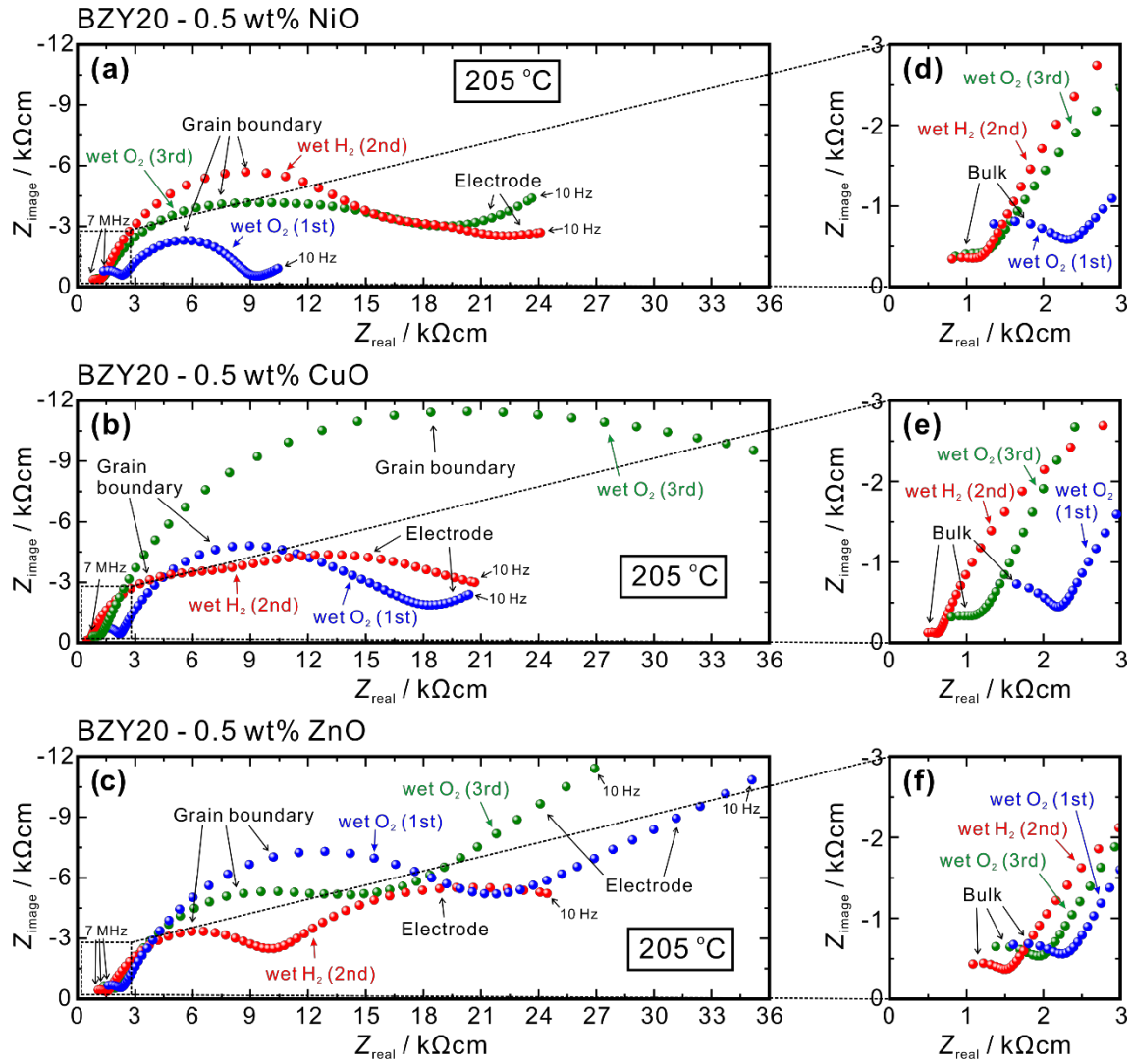
Fig. 6 Impedance spectra of BZY20 added nominally with 0.5 wt% NiO, CuO, or ZnO collected at 205 °C in wet O_2 (1st cycle), wet H_2 (2nd cycle) and wet O_2 (3rd cycle) in sequence. The partial pressure of water vapor was 0.05 atm.
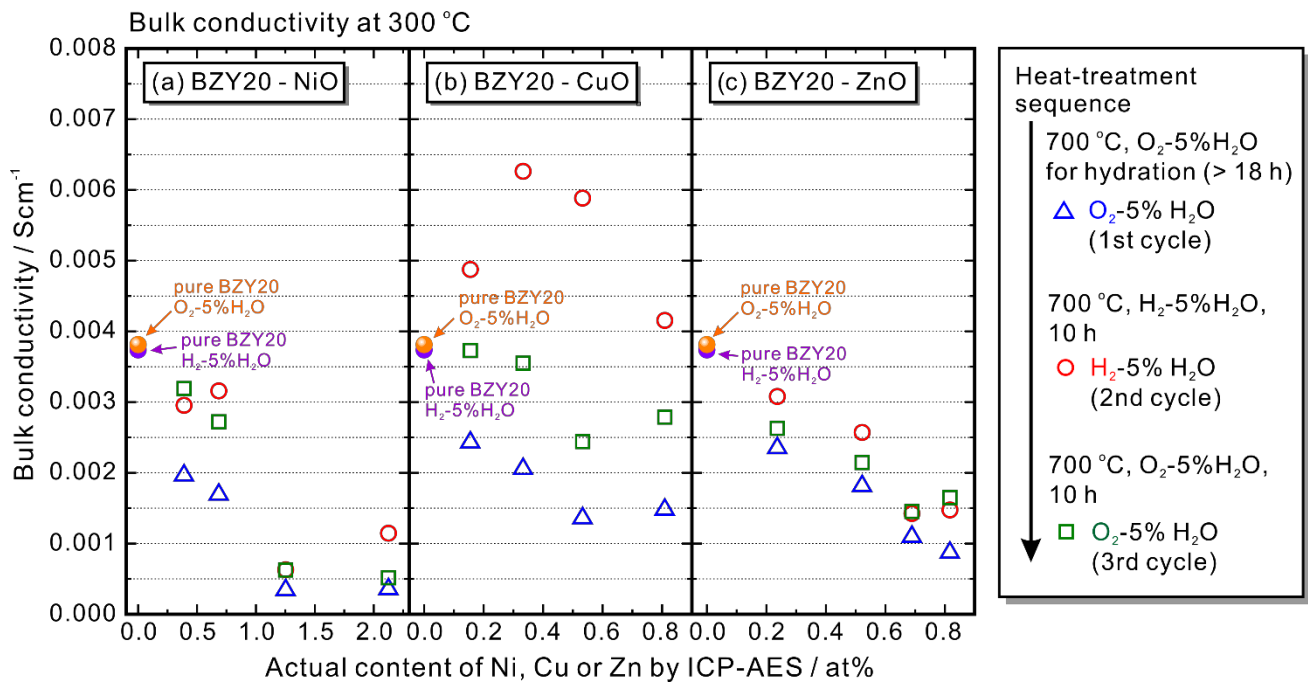
**Fig. 7** Bulk (intra-grain) conductivity at 300 °C of BZY20 added with various content of NiO, CuO or ZnO measured in wet O_2 (1st cycle), wet H_2 (2nd cycle) and wet O_2 (3rd cycle) in sequence. The partial pressure of water vapor was 0.05 atm.
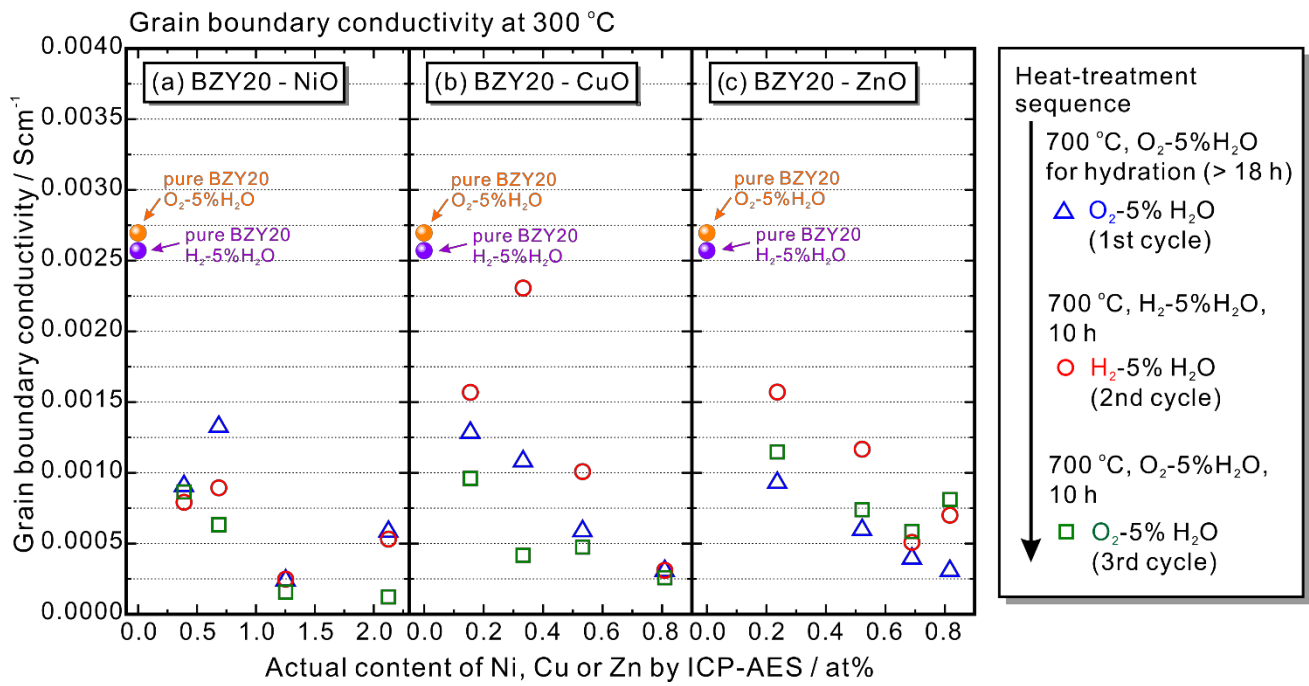
Fig. 8 Grain boundary conductivity at 300 °C of BZY20 added with various content of NiO, CuO or ZnO measured in wet O_2 (1st cycle), wet H_2 (2nd cycle) and wet O_2 (3rd cycle) in sequence. The partial pressure of water vapor was 0.05 atm.
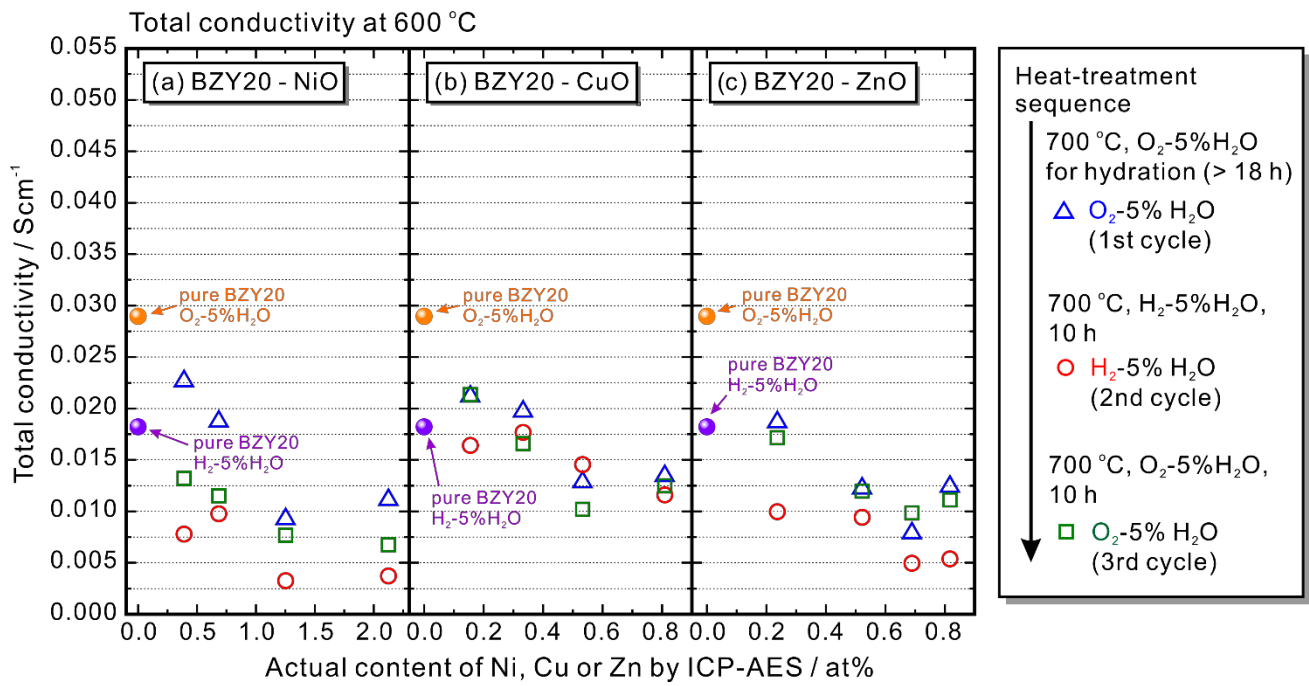
Fig. 9 Total conductivity at 600 ºC of BZY20 added with various content of NiO, CuO or ZnO measured in wet O_2 (1st cycle), wet H_2 (2nd cycle) and wet O_2 (3rd cycle) in sequence. The partial pressure of water vapor was 0.05 atm.
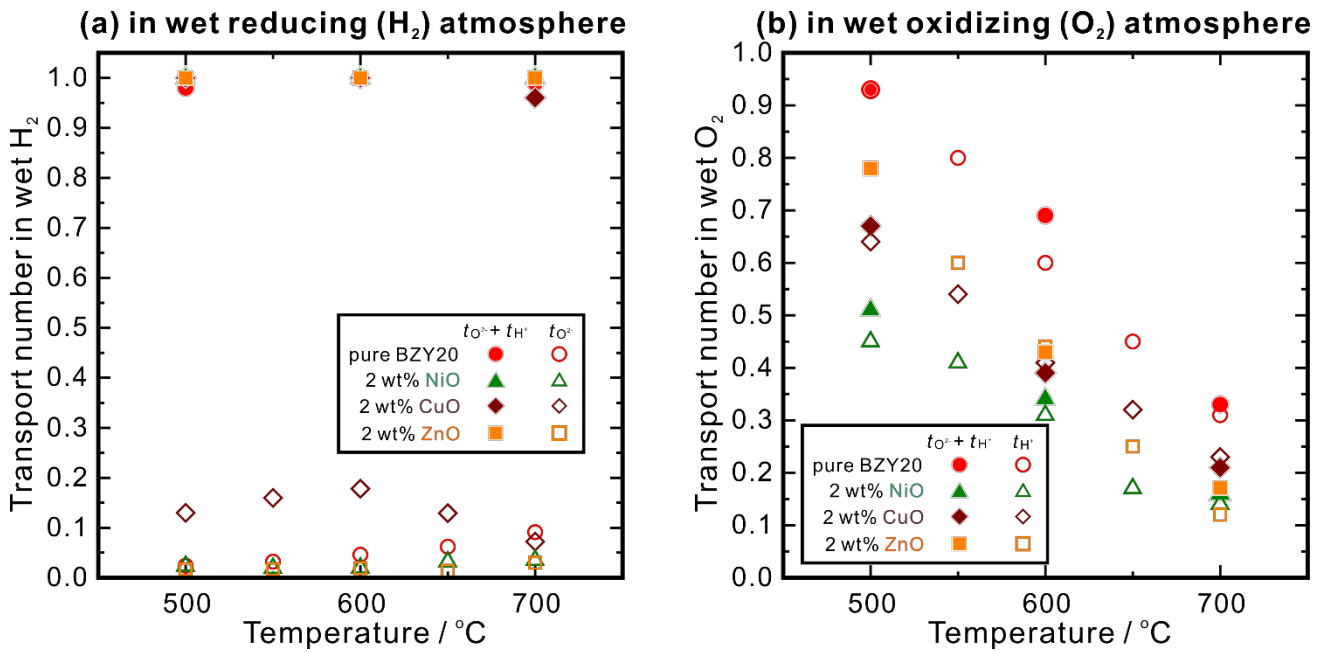
Fig. 10 Transport numbers of ionic conduction in pure BZY20 and those added nominally with 2 wt% NiO, CuO or NiO determined by the EMF method in (a) wet reducing (H_2), and (b) wet oxidizing (O_2) atmosphere. The transport number obtained in wet oxidizing (O_2) atmosphere were compensated by taking the effect from electrode polarization into consideration. In (a), the solid symbols are overlapped with each other since $t_{O^{2-}} + t_{H^+}$ is very close to unit for all the samples in wet hydrogen.
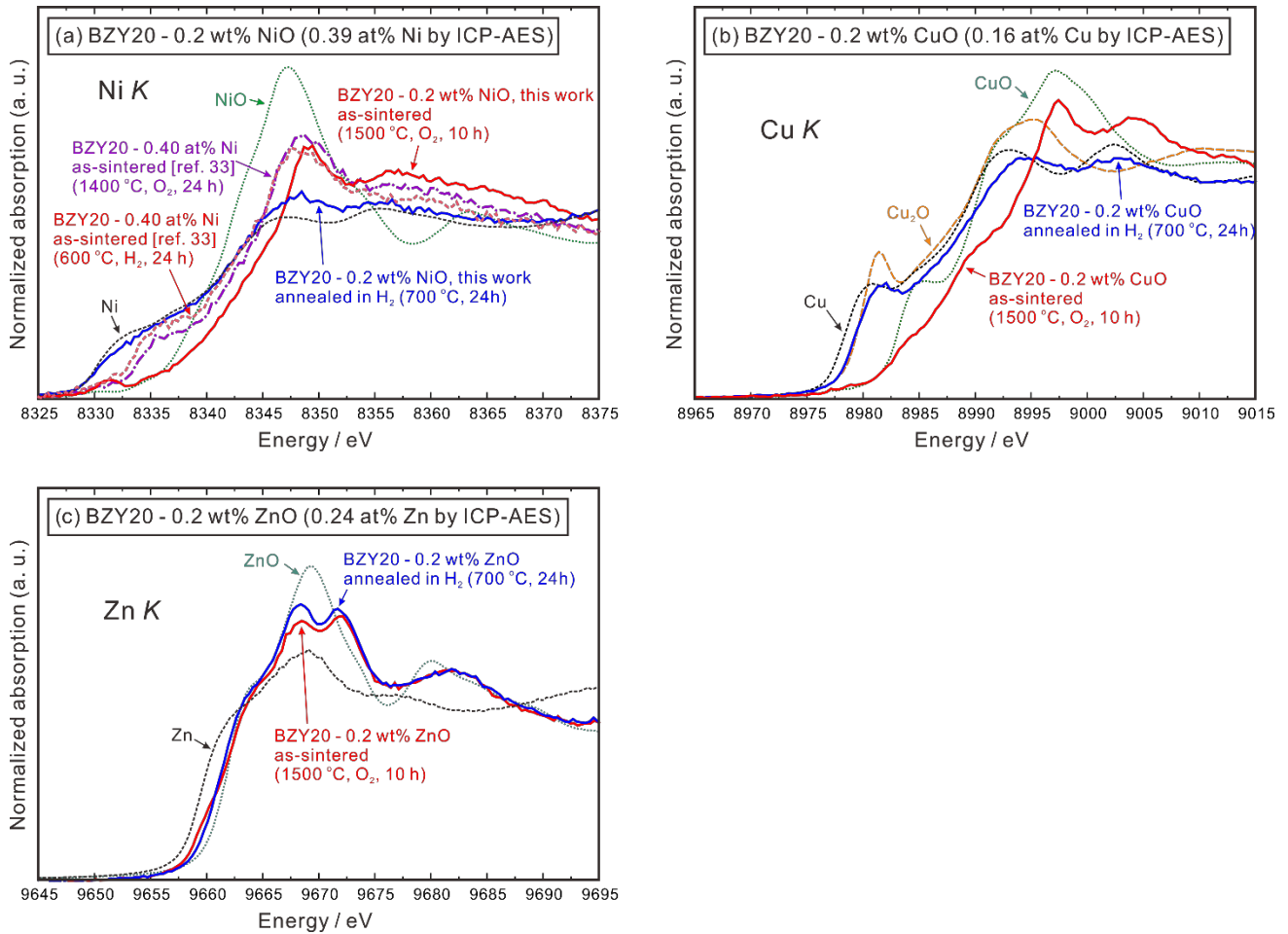
Fig. 11 (a) Ni *K*-edge XANES spectra of BZY20 – 0.2 wt% NiO, (b) Cu *K*-edge XANES spectra of BZY20 – 0.2 wt% CuO, and (c) Zn *K*-edge XANES spectra of BZY20 – 0.2 wt% ZnO collected at 20 K in a vacuum. All the samples were heat-treated at 1500 °C in oxygen for 10 h for sintering, and sequentially annealed in hydrogen at 700 °C for 24 h. Ni *K*-edge XANES spectra of BZY20 – 0.40 at% Ni (actual composition by ICP-AES) sintered at 1400 °C in oxygen for 24 h, and subsequently annealed in H₂ for 24 h, which were reported in our previous work [33], was also plotted in (a) for comparison.

Table 1 Reported performance at 600 °C of anode-supported PCFCs using BZY-based electrolytes. The thickness of the electrolyte layer was used in calculating the electrolyte conductivity. The performances of cells with the BZY electrolyte layer prepared by PLD [21, 30] were also listed for comparison.

Year for report	Reporters	Electrolyte			Anode	Cathode	Co-sintering temperature / °C	Cell performance	
		Nominal composition	Thickness / μm	Conductivity / Scm^{-1}				OCV / V	Peak power density / mWcm^{-2}
2010	Sun, *et al.* [20]	$BaZr_{0.8}Y_{0.2}O_{3-\delta}$	20	1.4×10^{-3}	$BaZr_{0.1}Ce_{0.7}Y_{0.2}O_{3-\delta}$ – 60 wt% NiO	$Sm_{0.5}Sr_{0.5}CoO_{3-\delta}$ – 40 wt% $Ce_{0.8}Sm_{0.2}O_{2-\delta}$	1400	1.014	70
2010	Pergolesi, *el al.* [21]	$BaZr_{0.8}Y_{0.2}O_{3-\delta}$	4	2.1×10^{-4}	$BaZr_{0.8}Y_{0.2}O_{3-\delta}$ – 26 wt% NiO	$BaCe_{0.9}Yb_{0.1}O_{3-\delta}$ – 50 wt% $La_{0.6}Sr_{0.4}Co_{0.2}Fe_{0.8}O_{3-\delta}$	By PLD	0.99	110
2011	Fabbri, *et al.* [22]	$BaZr_{0.7}Pr_{0.1}Y_{0.2}O_{3-\delta}$	20	1.5×10^{-3}	$BaZr_{0.8}Y_{0.2}O_{3-\delta}$ – 70 wt% NiO	$BaZr_{0.7}Pr_{0.1}Y_{0.2}O_{3-\delta}$ – 50 wt% $La_{0.6}Sr_{0.4}Co_{0.2}Fe_{0.8}O_{3-\delta}$	1500	0.93	81
2011	Bi, *et al.* [23]	$BaZr_{0.8}Y_{0.2}O_{3-\delta}$	30	2.7×10^{-3}	$BaZr_{0.8}Y_{0.2}O_{3-\delta}$ – 50 wt% NiO	$BaZr_{0.7}Pr_{0.1}Y_{0.2}O_{3-\delta}$ – 50 wt% $La_{0.6}Sr_{0.4}Co_{0.2}Fe_{0.8}O_{3-\delta}$	1400	0.95	51
2012	Sun, *et al.* [24]	$BaZr_{0.8}Y_{0.2}O_{3-\delta}$ - CaO	25	1.7×10^{-3}	$BaZr_{0.8}Y_{0.2}O_{3-\delta}$ – 60 wt% NiO	$BaZr_{0.8}Y_{0.2}O_{3-\delta}$ – 61 wt% $La_{0.6}Sr_{0.4}Co_{0.2}Fe_{0.8}O_{3-\delta}$	1400	0.96	72

2012	Xiao, et al. [25]	$BaZr_{0.8}Y_{0.2}O_{3-\delta}$	25	7.7×10^{-4}	$BaZr_{0.1}Ce_{0.7}Y_{0.2}O_{3-\delta}$ – 40 wt% NiO	$Sm_{0.5}Sr_{0.5}CoO_{3-\delta}$ – 30 wt% $Ce_{0.8}Sm_{0.2}O_{2-\delta}$	1450	0.97	55
2012	Luisetto, et al. [26]	$BaZr_{0.8}Y_{0.16}Zn_{0.04}O_{3-\delta}$	20	1.7×10^{-3}	$BaZr_{0.8}Y_{0.2}O_{3-\delta}$ – 60 wt% NiO	Pt	1450	0.93	47
2012	Liu, et al. [27]	$BaZr_{0.7}Nd_{0.1}Y_{0.2}O_{3-\delta}$	30	2.0×10^{-3}	$BaZr_{0.7}Nd_{0.1}Y_{0.2}O_{3-\delta}$ – 50 wt% NiO	$Ba_{0.5}Sr_{0.5}Co_{0.8}Fe_{0.2}O_{3-\delta}$	1450	0.99	105
2014	Sun, et al. [28]	$BaZr_{0.8}Y_{0.15}In_{0.05}O_{3-\delta}$	12	2.4×10^{-3}	$BaZr_{0.8}Y_{0.15}In_{0.05}O_{3-\delta}$ – 65 wt% NiO	$Sm_{0.5}Sr_{0.5}CoO_{3-\delta}$ – 40 wt% $Ce_{0.8}Sm_{0.2}O_{2-\delta}$	1400	0.99	81
2015	Shafi, et al. [29]	$BaZr_{0.76}Y_{0.2}Ni_{0.04}O_{3-\delta}$	12	2.1×10^{-3}	$BaZr_{0.8}Y_{0.2}O_{3-\delta}$ – 60 wt% NiO	$BaZr_{0.8}Y_{0.2}O_{3-\delta}$ – 70 wt% $PrBaCo_2O_{5+\delta}$	1450	1.01	240
2015	Duan, et al. [19]	$BaZr_{0.8}Y_{0.2}O_{3-\delta}$ – 1.0 wt% NiO	25	$\sim 0.9 \times 10^{-3}$	$BaZr_{0.8}Y_{0.2}O_{3-\delta}$ – 55 wt% NiO	$BaCo_{0.4}Fe_{0.4}Zr_{0.1}Y_{0.1}O_{3-\delta}$	1450	0.99	420
2015	Duan, et al. [19]	$BaZr_{0.8}Y_{0.2}O_{3-\delta}$ – 1.4 wt% CuO	25	unknown	$BaZr_{0.8}Y_{0.2}O_{3-\delta}$ – 55 wt% NiO	$BaCo_{0.4}Fe_{0.4}Zr_{0.1}Y_{0.1}O_{3-\delta}$	1450	0.99	470
2017	Bae, et al. [30]	$BaZr_{0.85}Y_{0.15}O_{3-\delta}$	2.5	2.78×10^{-3}	$BaZr_{0.85}Y_{0.15}O_{3-\delta}$ – 56 wt% NiO	$La_{0.6}Sr_{0.4}CoO_{3-\delta}$	By PLD	1.0	740
2017	Bi, et al. [31]	$BaZr_{0.8}Y_{0.2}O_{3-\delta}$	20	4.5×10^{-3}	$BaZr_{0.76}Y_{0.2}Ni_{0.04}O_{3-\delta}$ – 60 wt% NiO	$BaZr_{0.8}Y_{0.2}O_{3-\delta}$ – 50 wt% $PrBaCo_2O_{5+\delta}$	1400	0.99	267
2017	Dai [32]	$BaZr_{0.75}Y_{0.2}Pr_{0.05}O_{3-\delta}$	20	2×10^{-3}	$BaZr_{0.75}Y_{0.2}Pr_{0.05}O_{3-\delta}$ – 60 wt% NiO	$BaZr_{0.75}Y_{0.2}Pr_{0.05}O_{3-\delta}$ - $La_{0.6}Sr_{0.4}Co_{0.2}Fe_{0.8}O_{3-\delta}$	1400	0.93	124

Table 2 Average and local concentration of Ni, Cu, or Zn in BZY20 added nominally with 2 wt%

NiO, CuO, or ZnO, which were heat-treated at 1500 ºC in oxygen for 10 h, and sequentially annealed

in hydrogen for 48 h.   The average concentration is determined by ICP-AES measurement.   The

local concentration at intra-grain and grain boundary is determined by STEM-EDS point analysis.

Nominal composition	Cation ratio of Ni, Cu or Zn in relevant sample / at%				
	As-sintered (1500 ºC, O$_2$, 10h)			Annealed in H$_2$ (700 ºC, 48 h)	
	Average concentration	Intra-grain	Grain boundary	Intra-grain	Grain boundary
BZY20– 2 wt% NiO	2.13	1.93	2.50	1.92	2.34
BZY20 – 2 wt% CuO	0.81	0.48	2.03	0.24	0.38
BZY20 – 2 wt% ZnO	0.82	0.78	0.99	0.82	1.07